Molecular Neurobiology (2019) 56:2714–2727
https://doi.org/10.1007/s12035-018-1225-3

# Spatial Dynamics of Vascular and Biochemical Injury in Rat Hippocampus Following Striatal Injury and Aβ Toxicity

Zareen Amtul[1] · Carmen Frías[1] · Jasmine Randhawa[2] · David J. Hill[3,4] · Edith J. Arany[5]

Received: 14 January 2018 / Accepted: 5 July 2018 / Published online: 28 July 2018


## Abstract

The hippocampus, a brain region vital for memory and learning, is sensitive to the damage caused by ischemic/hypoxic stroke and is one of the main regions affected by Alzheimer's disease. The pathological changes that might occur in the hippocampus and its connections, because of cerebral injury in a distant brain region, such as the striatum, have not been examined. Therefore, in the present study, we evaluated the combined effects of endothelin-1-induced ischemia (ET1) in the striatum and β-amyloid (Aβ) toxicity on hippocampal pathogenesis, dictated by the anatomical and functional intra- and inter-regional hippocampal connections to the striatum. The hippocampal pathogenesis induced by Aβ or ET1 alone was not severe enough to significantly affect the entire circuit of the hippocampal network. However, the combination of the two pathological states (ET1 + Aβ) led to an exacerbated increase in neuroinflammation, deposition of the amyloid precursor protein (APP) fragments with the associated appearance of degenerating cells, and blood-brain-barrier disruption. This was observed mainly in the hippocampal formation (CA2 and CA3 regions), the dentate gyrus as well as distinct regions with synaptic links to the hippocampus such as entorhinal cortex, thalamus, and basal forebrain. In addition, ET1 + Aβ-treated rats also demonstrated protracted loss of AQP4 depolarization, dissolution of β-dystroglycan, and basement membrane laminin with associated IgG and dysferlin leakage. Spatial dynamics of hippocampal injury in ET1 + Aβ rats may provide a valuable model to study new targets for clinical therapeutic applications, specifically when areas remotely connected to hippocampus are damaged.

**Keywords** Beta-amyloid · Ischemia · Hippocampus · Striatum · Blood-brain barrier

## Introduction

The archicortical hippocampal formations, consists of five major intrahippocampal connections (fascia, dentate gyrus; DG, hilus, cornum ammonis (CA3-2), CA1, and subiculum), are regions of the brain most sensitive to ischemic damage. The hippocampal and retrohippocampal formations (presubiculum, parasubiculum, area retrosplenialis, and entorhinalis; entorhinal cortex) along with parahippocampal [1, 2] medial temporal lobe (MTL) [1, 2] and the islands of Calleja are part of a neuroanatomically well-defined cerebral limbic network involved in memory and learning behavior, particularly spatial information and associative memory processes [3–5]. In addition, the septohippocampal network of cholinergic neurons consists of the septal region (the medial and lateral septal nuclei, dorsomedial quadrant of the septum, and the nuclei of the horizontal (HDB) and vertical (VDB) limbs of the diagonal band of Broca) and the nucleus basalis of Meynert [6]. Animal, as well as clinical studies [7–10], revealed that the hippocampus is selectively vulnerable to ischemic and/or hypoxic stroke or the consequences of hypoperfusion [7], possibly due to its location and lack of vascularization [8]. Similarly, non-invasive imaging performed on multi-infarct dementia, Alzheimer's disease (AD), and Parkinson's disease with dementia patients demonstrated regional hypoperfusion

✉ Zareen Amtul
zareen.amtul@gmail.com

[1] Department of Anatomy and Cell Biology, University of Western Ontario, London N6A 5C1, Canada

[2] Department of Biology, University of Western Ontario, London N6A 5B7, Canada

[3] Departments of Medicine, Physiology and Pharmacology, and Pediatrics, University of Western Ontario, London N6A 5C1, Canada

[4] Lawson Health Research Institute, London, ON N6A 4V2, Canada

[5] Department of Pathology and Laboratory Medicine, University of Western Ontario, London N6A 5C1, Canada

most aggressively in the MTL, including the hippocampus, where the observed reduced cerebral blood flow (CBF) strongly associated with the extent of dementia [9]. Stroke during middle age profoundly increases the risk of AD [10]. It is possible that the stroke exacerbates the aging process by increasing the extent of inflammation, β-amyloid (Aβ) deposition, and neuronal and blood-brain barrier (BBB) loss [11, 12]. An underlying systemic vascular disorder, or, instead, the additive consequences of the AD and ischemic pathologies, might be responsible for the aggravated and earlier onset of impairments [11]. Therefore, inflammation, Aβ deposition, neurodegeneration, and altered BBB permeability point to a link between stroke and AD.

Similarly, we have provided insight into the critical pathological changes in neuroinflammation, endogenous β-amyloid deposition, neurogenesis, and cognition occurring in the hippocampus in a striatal endothelin-1 (ETI) model of ischemia and β-amyloid toxicity [13–18]. The ventral striatum is the brain region that showed β-amyloid (Aβ) deposition early in AD pathology by in vivo β-amyloid imaging [19]. Moreover, in the familial AD, the striatum is the first brain region where Aβ deposition starts [19]. Furthermore, intrahippocampal injections of ET1 [20] or Aβ25–35 [21] have been shown to result in neuronal degeneration and cell loss of the pyramidal cell layer [22, 23]. However, it is not understood how a brain region as anatomically distant as striatum can affect a nonischemic, remote region from the lesion core, such as the hippocampus. Therefore, we hypothesize that the biochemical and vascular exacerbation occurring in the hippocampus, due to the comorbid striatal ischemia and β-amyloid toxicity, are driven by anatomical and functional units, fibers, and inter-regional hippocampal synaptic connections to the ischemic area. The novelty of our study lies in its hypothesis that the progression to memory impairment might occur via functional connectivity so that an ischemic injury in the striatum, often affected in middle cerebral artery (MCA) localized strokes, could exacerbate deleteriously pathology in interconnected regions. Spatial dynamics of hippocampal injury in ET1 + Aβ rats may provide a valuable model to study new targets for clinical therapeutic applications, specifically when areas remotely connected to hippocampus are damaged [24]. Hence, in the present investigation, we examined neuroinflammation, β-amyloid deposition, microvasculature, and BBB alteration to determine the role of hippocampal-specific biochemical and vascular patterns driven by connectivity to striatum in comorbid conditions of cerebral ischemia and β-amyloid toxicity.

Enhanced appreciation of the connectivity pattern of the structural links of biochemical and vascular injury among distinct anatomical and functional hippocampal units after ET1 and/or Aβ toxicity could provide insight into the pathogenic mechanisms and a new rationale for the design of therapeutics for demented patients.

## Materials and Methods

### Animal, Treatment, and Tissue Preparation

All animal protocols were carried out according to the guidelines of the Animal Use and Care Committee of the Western University (approval ID: 2008-113). Male Wistar rats (240–310 g) were anesthetized using 1.8% isoflurane. The animals were positioned in a stereotaxic apparatus (David Kopf) with the incisor bar below the interaural line, set at 3.3 mm. Body temperatures were maintained at 37 °C. To insert the Hamilton syringe (30 gauge), small burr holes were drilled in the parietal bone. There were four groups of animals ($n = 6$ for each group). To model striatal ischemia (ET1 group), 60 pmol endothelin-1 (ET1; Sigma-Aldrich, Oakville, ON) per 3 μL (dissolved in saline) was injected (single time) into the right striatum through the Hamilton syringe (anterior/posterior + 0.5 mm, medial/lateral − 3.0 mm relative to bregma, and dorsoventral − 5.0 mm below dura). The well-established rat model of β-amyloid toxicity (Aβ group) was used [21, 22]. Briefly, a bilateral injection of Aβ25–35 (50 nmol/10 μL of saline) (Bachem, Torrance, California) was made into the lateral ventricles (anterior/posterior − 0.8 mm, mediolateral ± 1.4 mm relative to bregma, and dorsoventral − 4.0 mm below dura). Aβ25–35 peptide is likely generated endogenously by enzymatic proteolysis of Aβ40 [25, 26], and due to its high hydrophobic amino acids content tends to aggregate more than the Aβ42 peptide. It has been identified in AD brains in the core of senile plaques, extracellular neurofibrillary tangles, and degenerating CA1 hippocampal neurons of AD patients, but not in control subjects [26]. For rats getting both bilateral intracerebroventricular (ICV) Aβ25–35 injections and unilateral ET1 (ET1 + Aβ group) injections, the Aβ25–35 peptide injection into the lateral ventricles was followed by the striatal ET1 injection. The control rats (control group) went through the identical steps but with saline injections. The Paxinos and Watson [27] atlas was used to determine all stereotaxic coordinates. Following ET1, Aβ25–35, or saline injections, the syringe was left in situ for 3 min before being removed slowly to avoid a backward flow. After suturing the wound, all rats received 30 μg/kg buprenorphine injection subcutaneously and an injection of 20 μl (50 mg/ml stock) enrofloxacin antibiotic (Baytril, Bayer Inc., Canada) intramuscularly. Four weeks after surgery, rats were euthanized with pentobarbital (160 mg/kg, i.p) and transaortically perfused, first with heparinized phosphate-buffered saline (PBS) followed by 4% paraformaldehyde (pH 7.4). The brains were immediately removed, post-fixed in 4% paraformaldehyde for 24 h, and cryoprotected by immersion in 30% sucrose at 4 °C for 36 h. Gross cerebral hemorrhage was noticed in three ET1 and two Aβ rats, which were discarded and repeat experiments performed. No hemorrhages were detected in any of the control rats.

## Histology

Immunohistochemistry was performed on serial, coronal sections of the entire brain, 35 μm in thickness using a sliding microtome (Tissue-Tek Cryo3, USA) as described [13, 14, 17, 18]. Sections were stained with the following antibodies: 4G8 (Signet, 9220-10, 1:1000) for amyloid precursor protein (APP) fragments including Aβ; OX6 (BD Pharmingen, 554,926, 1:1000) for MHCII antigens expressed by the microglia; anti-basement membrane (BM)-laminin (Sigma, L 9393, 1:1000) as an indicator of the BM leakage rather than a vascular marker; anti-SMI71 (Covance, SMIR, 1:2000) which is a specific endothelial barrier antigen (EBA) located in mature endothelial cells of the blood vessels with functional BBB [28], anti-IgG for vascular permeability (Invitrogen, A21209, 1:500); anti-glial fibrillary acidic protein (GFAP, Sigma, G3893, 1:1000) for active astrocytes; anti-aquaporin-4 (AQP4, Chemicon, AB2218, 1:1000) for water channel protein; anti-matrix metalloproteinase9 (MMP9; Millipore, AB19016, 1:1000) and anti-β-dystroglycan (β-DG; Leica B-DG-CE-S, 1:200) to demonstrate astrocytic anchoring around the cerebral endothelium; anti-dysferlin (Abcam, ab 75,571, 1:200) to detect leakage of inflammatory infiltrates; anti-NeuN (Chemicon, MAB377, 1:200) to stain neuronal nuclei; and FluoroJade B (FJB) (Chemicon Int., 0.0004%) to visualize degenerating cells. For fluorochrome FJB staining, mounted sections were placed in 0.06% potassium permanganate solution for 15 min, in 0.0004% FJB (Chemicon Int.) solution for 20 min, rinsed in distilled water, cleared in xylene, and coverslipped using Depex.

## Analyses

The angioarchitecture of the hippocampal gray matter and microvasculature between 0.48 and − 5.8 mm anterior to posterior was selected as the region of interest for investigation under light and fluorescence microscope. A Leica Digital Camera DC 300 (Leica Microsystems Ltd., Heerbrugg, Switzerland) attached to Leitz Diaplan microscope and Leica IM50 software was used to acquire the images. Digitized photomicrographs obtained as TIFF files using a 10x objective and brought to the same sharpness and contrast level using the IM50 software. Manual stereologic counting method was employed to count and identify the numbers and locations of cells unequivocally on the basis of positive labeling by visual inspection within hundreds of microscopic fields-of-view. Six non-neighboring brain slices were analyzed from each rat, starting from the anterior basal forebrain level (0.48 mm) to the posterior hippocampal level (− 5.8 mm from the bregma) with 210 μm distance. Six fields were studied in each hippocampal region. Cellular or vascular densities (expressed as the number of cells or vessels in the optical field/mm$^2$) were quantified as the arithmetic mean of the six slices in ipsilateral hemisphere of each rat divided by the total area of the region (6.28 mm). Two separate individuals blinded to the study group undertook each quantification. Microvessels were counted using stereoscopic method [29] at 10x magnification from six randomly placed fields per hippocampal region per slice. Segments from each microvessel were counted separately. All values were presented as a mean ± standard error of the mean (S.E.M.) and were analyzed using one-way ANOVA followed by post hoc Dunnett's tests. The significance level was set at $p \leq 0.05$.

# Results

## Thalamic Pathology

The ET1 and ET1 + Aβ rats exhibited several characteristic features of a degenerated brain. First, IgG leakage in Fig. 1(a) showed the size of the ischemic lesion in the ipsilateral striatum in ET1 and ET1 + Aβ rat brains compared to its absence in control and Aβ rats. In thalamus, IgG leakage (Fig. 1(b)) and the number of ramified microglia (Fig. 1(c) OX6) appeared not only in the ipsilateral side but also spread to the contralateral side in both ET1 and ET1 + Aβ rats, with an increased trend in ET1 + Aβ-treated animals compared to ET1 rats but significantly more than the Aβ rats ($p < 0.01$). Next, we examined the levels of endogenous APP fragments, as ET1 injection elevates the deposition of APP fragments, including β-amyloid, in the brain. APP fragments-positive neurons in the ET1 + Aβ thalamus weakly exhibit deficient dendritic and axonal branching compared to the ET1 rats ($p = 0.07$) but did so more when compared to Aβ rats ($p \leq 0.001$) (Fig. 1 APP fragments). To examine cellular degeneration, we used FJB (polyanionic fluorescein derivative) that has been reported to stain dying neuronal cells in cases of acute insult [30] and label astrocytes and microglia [31] at some stage in a chronic neurodegenerative course. In the ventral posteromedial (VPM) and ventral posterolateral (VPL) nuclei, ET1 + Aβ rats did not show a significant decrease in cell survival compared to ET1 but did so when compared to Aβ rats ($p \leq 0.001$) (Fig. 1 FJB). In ET1 and ET1 + Aβ animals, MMP9 showed a strong astrocytic expression in the area of astrogliosis with more in ET1 rats compared to ET1 + Aβ brains, while in control and Aβ rats, MMP9 showed neuronal expression. Correspondingly, the area surrounding the astrogliosis showed a fragile network of microvessels with stabilized β-DG expression (Fig. 1 MMP9/β-DG) and functional BBB (SMI) (Fig. 1 Lm/SMI). MMP9 is protective when expressed by astrocytes and mediates BBB repair by stabilizing β-DG in

neurovascular remodeling and regeneration process [32]. This may represent an attempt by the brain to restore the broken BBB and sustain CBF, 4 weeks after injury. In contrast to laminin (Lm) staining, SMI staining did not differ in ET1 + Aβ rats compared to ET1 rats ($p > 0.05$) but was sparingly observed when compared to Aβ rats ($p = 0.01$). MMP9 and laminin-like molecules could also be seen in neurons throughout the control and Aβ rats as well as in the non-injured regions of ET1 and ET1 + Aβ rats. ET1 + Aβ rats tended to show a resulting weakly increase in the leakage of dysferlin-positive inflammatory infiltrates compared to ET1 ($p = 0.06$) which became definitive in Aβ rats ($p < 0.001$) (Fig. 1 dysferlin). Weak GFAP (red) expression in control and Aβ rats ($p = 0.005$ compared to ET1 + Aβ rats) steadily developed fourfold into glia scar in ET1 ($p = 0.054$ compared to ET1 + Aβ rats) and ET1 + Aβ rats. The distribution of granulated AQP4 channels (green) was highly polarized in the astrocytic end-feet cell membranes around vascular endothelial cells in control and Aβ rats compared to ET1 and ET1 + Aβ rats. In contrast, in the ET1 + Aβ rats, a highly significant increase in AQP4 staining intensity was found compared to Aβ ($p < 0.001$) and ET1 ($p < 0.001$) animals associated with the redistribution of polarized expression of AQP4 from astrocytic foot processes to astrocytic parenchymal membrane [33], as shown in dual immunofluorescent images of AQP4 and GFAP colocalization. Depolarization of AQP4 expression on astrocytic end-feet (merged images) is associated with its role in the resolution of vasogenic edema (Fig. 1 AQP4/GFAP). In addition, the response of astrocytes to injury is manifested by their increased proliferation and size along with cytoplasmic processes elongation [34]. ET1 ($p < 0.05$) and ET1 + Aβ ($p = 0.05$) rats also displayed a decisive decrease in NeuN stained pyknotic neurons (resembling apoptotic cells) compared with control rats (Fig. 1 NeuN).

## Entorhinal Cortex Pathology

Entorhinal cortex (Fig. 2(a)) showed a substantial and significant increase in neuroinflammation in Aβ, ET1, and ET1 + Aβ rat brains compared to none in control rats (Fig. 2 OX6). Not only were there significantly greater numbers of microglia in the ET1 + Aβ rats compared to Aβ ($p = 0.001$) rats, but the microglia were also found in clusters, with plump somas, and intense immunoreactivity throughout the soma and processes, indicating a profound increase in intracellular MHC II expression. Neuroinflammation was also accompanied by the significant deposition of APP fragments producing (Fig. 2 APP fragments) and FJB-positive cells (Fig. 2 FJB) in ET1 + Aβ rats compared to Aβ rats (Aβ $p = 0.003$, FJB $p = 0.002$), while an increased trend was found compared to ET1 rats. According to their morphology and distribution pattern, APP fragments-positive cells appeared to be degenerating neurons. A network of BM-laminin protein, that demonstrates the leakage of laminin across the compromised BM and BBB, was also seen across the groups with an increased trend in ET1 + Aβ rats compared to control, Aβ, and ET1 rats (Fig. 2 Lm/SMI).

## Basal Forebrain Pathology

Septohippocampal (Shi) and lateral septal (LSD) nuclei demonstrated increased numbers of ramified microglial cells in Aβ ($p = 0.004$) and ET1 + Aβ ($p = 0.055$) rats compared to control and ET1 brains, respectively (Fig. 3(a)). Similarly, APP fragments stained cells were seen within the inflamed microvessels in all the tested animals with substantially more in Aβ ($p \leq 0.01$) and ET1 + Aβ ($p > 0.05$) rats compared to control and ET1 brains, respectively (Fig. 3(a) APP fragments). We found a significant number of FJB-positive degenerative cells, with a distinct microglial morphology and distribution pattern with substantially more in Aβ ($p = 0.05$) and ET1 + Aβ animals ($p = 0.007$) compared to control brains (Fig. 3(a) FJB), indicating that 3 weeks after the surgery, some of the microglial cells were on the verge of degeneration. Similarly, medial septal nucleus (MS) showed increased extravasation of IgG protein from the inflamed microvessels (Fig. 3(b) IgG). The MS, VDB, HDB, and medial forebrain bundle (MFBB) also showed a general increase in APP fragments stained cells that from morphology and appearance look like neurons with more in Aβ and ET1 + Aβ rats compared to ET1 and control brains (Fig. 3(b) APP fragments). In brain regions comprised of ventral pallidum (VP), HDB, anterior amygdala area (AAV), and islands of Calleja (ICj) OX6 antibody showed dense extracellular deposits instead of ramified microglia with significantly more in ET1 + Aβ rats compared to Aβ ($p = 0.035$) but not compared to ET1 rats (> 0.05) (Fig. 3(c) OX6). Interestingly, the microglia were observed in the vicinity of microvessels, whereas Aβ antibody showed deposition of β-amyloid fragments around microvessels and in cells with the appearance of neurons and astrocytes. Insets showed APP fragments-positive neuronal and astrocytic cells surrounding the leaky microvessels (Fig. 3(c) APP fragments). FJB-positive cells in this region also showed distinctive microglial morphology with more in ET1 + Aβ compared to Aβ ($p = 0.01$) but not compared to ET1 rats ($p = 0.058$) (Fig. 3(c) FJB). SMI staining colocalized almost completely with BM-laminin staining in Aβ rats except in inflamed and dilated microvessels of ET1 and ET1 + Aβ rats, suggesting a weakly greater BBB loss in ET1 + Aβ rats compared to ET1 ($p = 0.06$) rats but significantly more compared to Aβ ($p = 0.003$) rats. ET1 and ET1 + Aβ rats also showed uneven, locally thickened BM continuous with the non-affected and normal BM (Fig. 3(c) Lm/SMI).

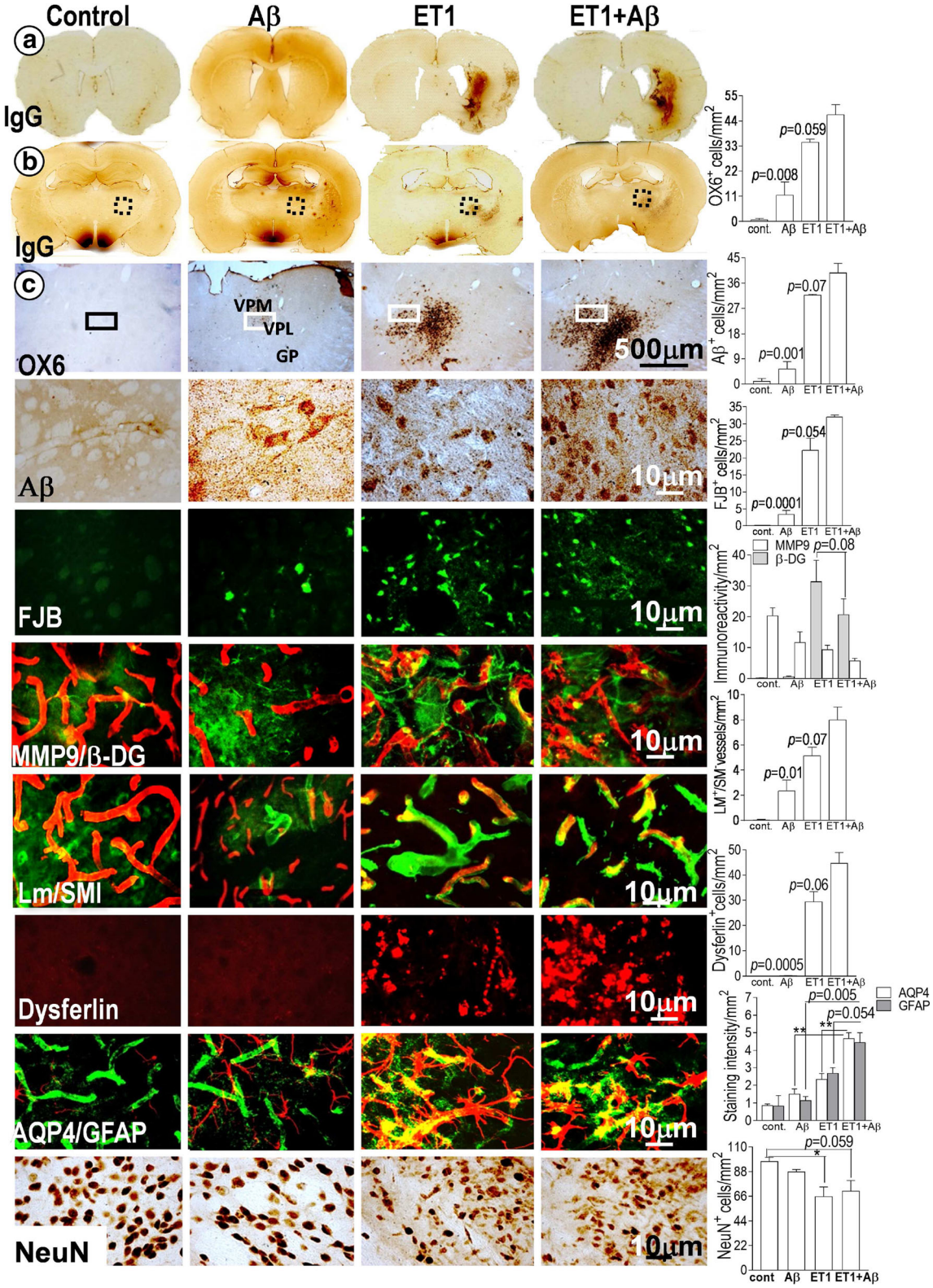


## Cornu Ammonis Pathology

CA1 (a), CA2 (b), and CA3 (c) showed ramified microglial cells in Aβ, ET1, and ET1 + Aβ rats (Fig. 4(a–c)). While CA1 showed significantly more APP fragments and FJB-positive cells in ET1 + Aβ rats compared to Aβ (Aβ $p = 0.03$, FJB $p = 0.01$) rats, in CA2, ET1 + Aβ rats demonstrated fewer number of Aβ fragments-positive cells compared to ET1 rats, due to the comparatively more loss of neuronal cells in these animals (Fig. 4(b) APP fragments). Similarly, a higher number of

◀ **Fig. 1** Thalamic pathology: representative coronal sections stained with an IgG antibody show striatal lesion at bregma level 0.48 mm (a) and a thalamic lesion at bregma level − 2.3 mm (b). Low-resolution images (c) at bregma level − 2.3 mm show thalamic pathology in ventral posteromedial (VPM) and ventral posterolateral (VPL) nuclei. Globus pallidus (GP) is shown to orient the readers. The dotted rectangles in b indicate the region of the high magnification images. High-resolution immunostaining indicates ramified microglia (OX6), APP fragments including β-amyloid (Aβ), FJB-positive cells (FJB), MMP9-(green) positive astrocytes (MMP), β-DG (red)-positive vessels (β-DG), laminin (green)-positive microvessels (Lm), SMI (red)-positive vessels (SMI), dysferlin-positive inflammatory infiltrates (dysferlin), AQP4 (green) depolarization (AQP4), GFAP- (red) positive astrocytes (GFAP), and NeuN-positive neuronal cells (NeuN) in the ipsilateral thalamus. Plots show a quantitative analysis of OX6, Aβ, FJB, BM-laminin, SMI, MMP9, β-DG, dysferlin, AQP4, GFAP, and NeuN immunoreactivity in the control, Aβ, ET1, and ET1 + Aβ rats, $*p < 0.05$; $**p < 0.01$.

OX6- and FJB-positive cells in the CA2 region of ET1 rats compared to ET1 + Aβ rats and Aβ rats showed that the injury matures more rapidly in ET1 rats compared to other treatments (Fig. 4(b) OX6 and FJB). The CA3 subregion of ET1 + Aβ rats was characterized by a comparably larger injury in contrast to CA1 and CA2 subregions. The majority of microglial cells in the CA3 region were found close to the fimbria (Fig. 4(c) OX6). In CA3, ET1 + Aβ rats resulted in a general increase in APP fragments stained cells compared to Aβ ($p = 0.01$) and ET1 ($p = 0.05$) rats, close to the pyramidal cell layer that from morphology and appearance look like neurons with few processes and stout soma (Fig. 4(c) APP fragments). Similarly, we found a significant number of degenerating cells in ET1 + Aβ brains compared to Aβ ($p = 0.001$) but not compared to ET1 ($p = 0.064$) brains with a distinct microglial morphology (Fig. 4(c) FJB). Inflamed microvessels exhibited less SMI immunoreactivity, and at higher magnification revealed punctate immunoreactivity along the individual vessel walls which showed a robust BM-laminin staining, particularly evident in the hippocampal CA3 region of ET1 + Aβ rats significantly compared to Aβ ($p = 0.01$) but weakly compared to ET1 rats ($p = 0.056$) (Fig. 4(c) Lm/SMI).

## Dentate Gyrus Pathology

The number of ramified microglia appeared not only in the ipsilateral DG but also spread to the contralateral side in both

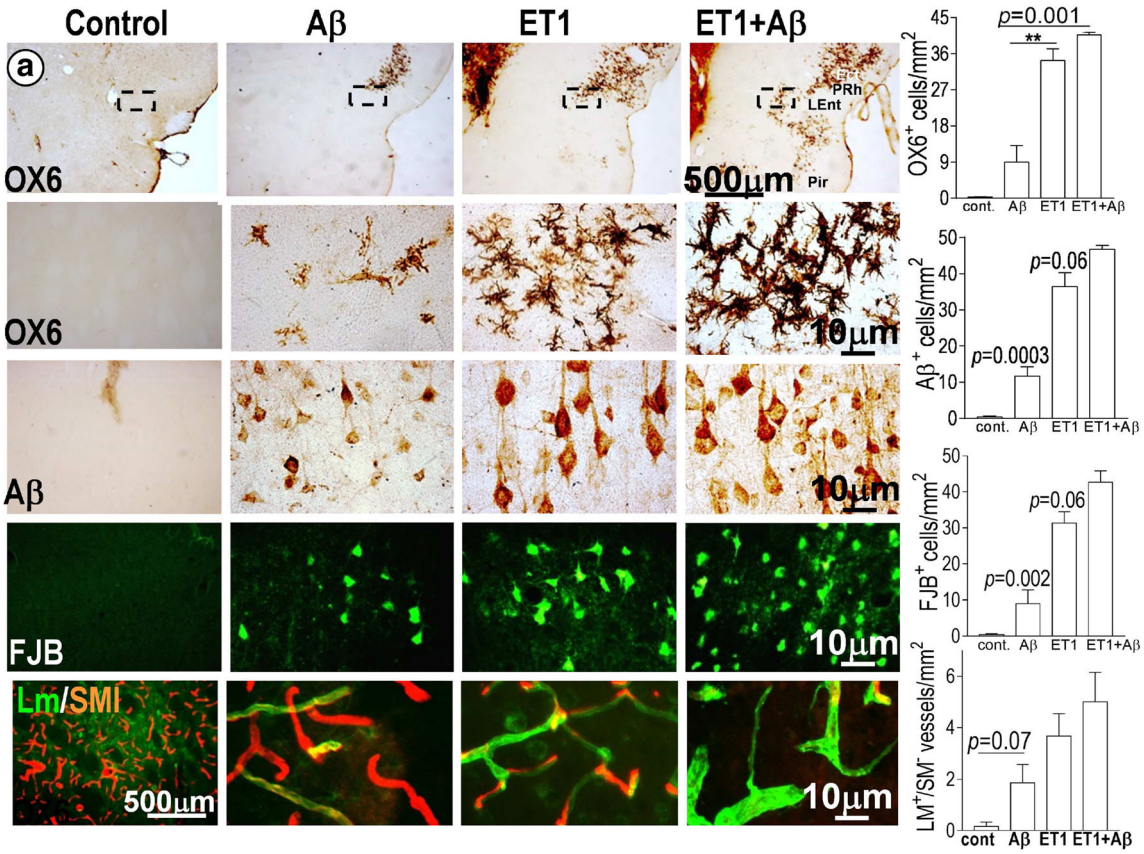


**Fig. 2** Entorhinal cortex pathology: low-resolution images at bregma level − 2.8 mm stained with OX6 antibody show cortical pathology in the ecto (Ect), peri (PRh), entorhinal (LEnt), and piriform (Pir) (a) cortices of control, Aβ, ET1, and ET1 + Aβ rats. The dotted rectangles indicate the region of the high magnification images. High-resolution immunostaining indicates ramified microglia (OX6), APP fragments including β-amyloid (Aβ), FJB-positive cells (FJB), laminin (Lm)- and SMI- (SMI) positive microvessels in the ipsilateral entorhinal cortex. Plots show a quantitative analysis of OX6, Aβ, FJB, BM-laminin, and SMI immunoreactivity in the control, Aβ, ET1, and ET1 + Aβ rats, $**p < 0.01$

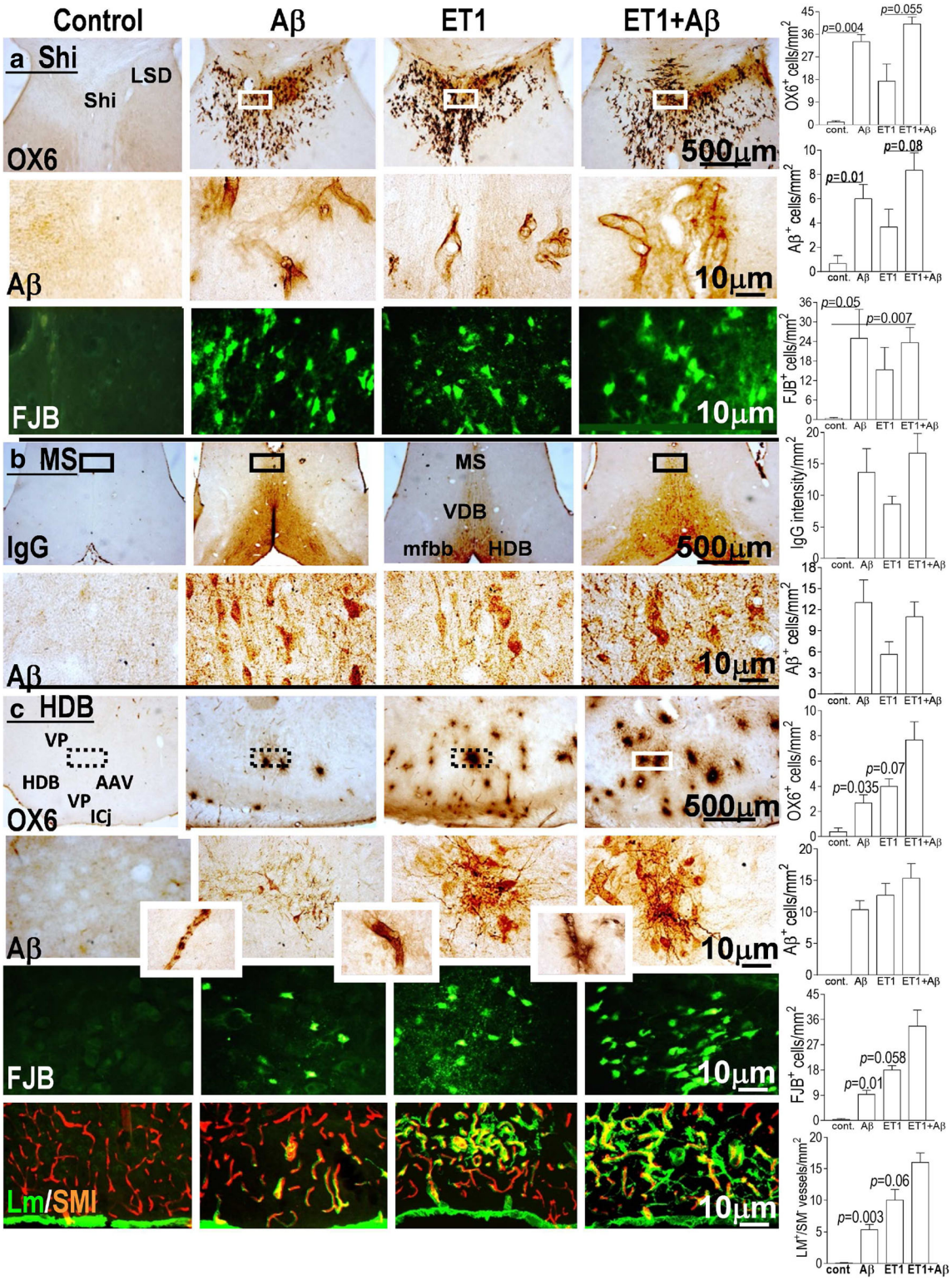


**Fig. 3** Basal forebrain pathology: low-resolution sections at bregma level 0.2 mm stained with OX6 and IgG antibodies show septohippocampal (Shi), lateral septal nucleus (LSD) (a) and medial septal nucleus (MS), vertical (VDB), horizontal (HDB) diagonal band of Broca, and medial forebrain bundle (mfbb) (b) pathology. While images at bregma level − 0.26 mm stained with OX6 antibody show HDB, ventral pallidum (VP), anterior amygdala area (AAV), and islands of Calleja (ICj) (c) pathology in control, Aβ, ET1, and ET1 + Aβ rats. The solid and dotted rectangles indicate the region of the high magnification images. High-resolution immunostaining indicates APP fragments including β-amyloid (Aβ), FJB-positive cells (FJB), IgG leakage (IgG), BM-laminin (Lm) and SMI (SMI)-positive microvessels in the ipsilateral basal forebrain of control, Aβ, ET1, and ET1 + Aβ rat brains. Plots show a quantitative analysis of OX6, Aβ, FJB, BM-laminin, and SMI immunoreactivity in the control, Aβ, ET1, and ET1 + Aβ rats.

ET1 and ET1 + Aβ rats (Fig. 5(a) OX6). Increased immunostaining for morphologically neuronal cells expressing APP fragments, including β-amyloid, was also increased with substantially more in ET1 + Aβ rats compared to Aβ ($p = 0.03$) and ET1 ($p = 0.05$) rats (Fig. 5 APP fragments). DG showed overall decreased cell survival in ET1 + Aβ rats ($p = 0.05$) compared to control, Aβ, and ET1 rats (Fig. 5 FJB). SMI staining colocalized almost completely with BM-laminin staining except in inflamed microvessels with IgG leakage, suggesting a BBB loss in those vessels, more obvious in ET1 + Aβ rats compared to Aβ ($p = 0.03$) and ET1 ($p = 0.06$) rats (Fig. 5 Lm/SMI). Most notably, the IgG leakage in the granular cell layer of DG (dotted line in Fig. 5 IgG) with reduced SMI immunoreactivity (Fig. 5 Lm+/SMI−) on microvessels suggests a decrease in the expression of tight junction protein at those sites with a resulting elevated BBB permeability. Similarly, as shown by us throughout, an increased number of OX6 stained cells was associated with reduced SMI staining in the hippocampus and its connected pathways. This finding refers to a potential association between vascular alterations and inflammation in the present study.

### Fornix and Hippocampal Commissure Pathology

OX6 staining showed a general increase in the number of microglial cells concentrated ipsilaterally in the ET1 and bilaterally in the hippocampal fimbria (Fig. 6(a, b)) and hippocampal commissure (Fig. 6(c) OX6) of Aβ and ET1 + Aβ rats with significantly more in ET1 + Aβ rats compared to Aβ (fi $p = 0.01$, df $p = 0.009$) rats. We found an increase in FJB staining in the hippocampal commissure with relatively more in ET1 + Aβ rats significantly compared to Aβ ($p = 0.003$) and weakly compared to ET1 ($p = 0.06$) rats (Fig. 6 FJB). A progressive shrinkage of the hippocampus and hippocampal fimbria (which is a prominent band of white matter) could also be appreciated in Fig. 6(a, b).

## Discussion

In the present investigation, we show that a single icv bilateral injection of Aβ and unilateral intrastriatal injection of ET1 provoked substantial biochemical alterations in the cellular and vascular anatomy of the hippocampus that provides an etiology link between AD and ischemia. Largely MTL [1] (including thalamus and entorhinal cortex), intrahippocampal subdivisions, CA3-2, and DG, fornix, hippocampal commissure, and basal forebrain were affected. Conversely, the hippocampal pathogenesis/atrophy induced by ET1 or Aβ toxicity alone was not severe enough to significantly affect the entire circuit in a hippocampal network.

While striatum and thalamus were the major injury sites in ET1 and ET1 + Aβ rats, degenerative changes were also observed in distant regions [35] with synaptic links to the striatal and thalamic lesions such as hippocampal subfields CA2, CA3, which are intimately unidirectionally connected to the reward-processing network of the ventral striatum (nucleus accumbens) [36, 37]. Similarly, anterior nuclei of the thalamus have direct connections to the hippocampus through fornix. Alternatively, cellular and vascular disruption observed in entorhinal cortex may also be the epicenter of damage seen in DG, CA1, and CA3, as the perforant pathway projection [1] from the entorhinal cortex directly innervates these hippocampal subdivisions [2, 38]. While thalamic deterioration in early AD stages is controversial [39, 40], we observed an early sign of degeneration in the thalamus of ET1 + Aβ rats with elevated astroglial expression, vascular degeneration, BBB disruption, and the presence of pyknotic neurons. Conversely, we observed a decrease in thalamic neuronal loss in Aβ rats compared to ET1 and ET1 + Aβ rats. This points to an aggravated drift towards AD pathology when it occurs comorbidly with ischemia. Disruption of thalamus-hippocampal connections leads to short-term and working memory impairment [41–43].

Similarly, origination of extrinsic afferent projections from the medial septum and basal forebrain to the CA1 (*reviewed in* [44]) as well as the fornix that connects the hippocampus with the cholinergic septal nuclei and VDB nuclei [6] may cause additional damage to CA1 region, provided the damage is severe enough at its site of origin. This connectivity between basal forebrain and hippocampus may be one of the contributing factors for the cellular and vascular degeneration seen in the hippocampus of ET1 and ET1 + Aβ rats and pointing to yet another intriguingly similar pathology between ischemia and AD [45]. Hypoactivity of septohippocampal cholinergic neuronal projections is an early AD pathology (*reviewed in* [45]).

DG and CA3 were affected the most (sparing CA1 and CA2), because mossy fibers, which are the axons of the granule cells of DG terminate in the CA3 subfield. The integrity of these connections is essential for episodic memory, which is primarily affected in AD [46]. The present study did not find any support to verify the vascular theory of CA1 vulnerability [47, 48]. Perhaps, the reported massive regeneration of neurons in CA1 of rat hippocampus after ischemia [49] also made them less susceptible to ischemia and/or Aβ toxicity in the present study. On the contrary, the higher capillary density of CA3 may be related to its increased vulnerability. Increased capillary density results in the shorter average distance between the capillary lumen and surrounding neurons. Therefore, neurons in CA3 region are adapted to faster delivery of oxygen and nutrients and as a result to be more susceptible to ischemia and/or Aβ insults in the current study.

The hippocampal divisions greatly affected by various deleterious biochemical changes due to the damage to their

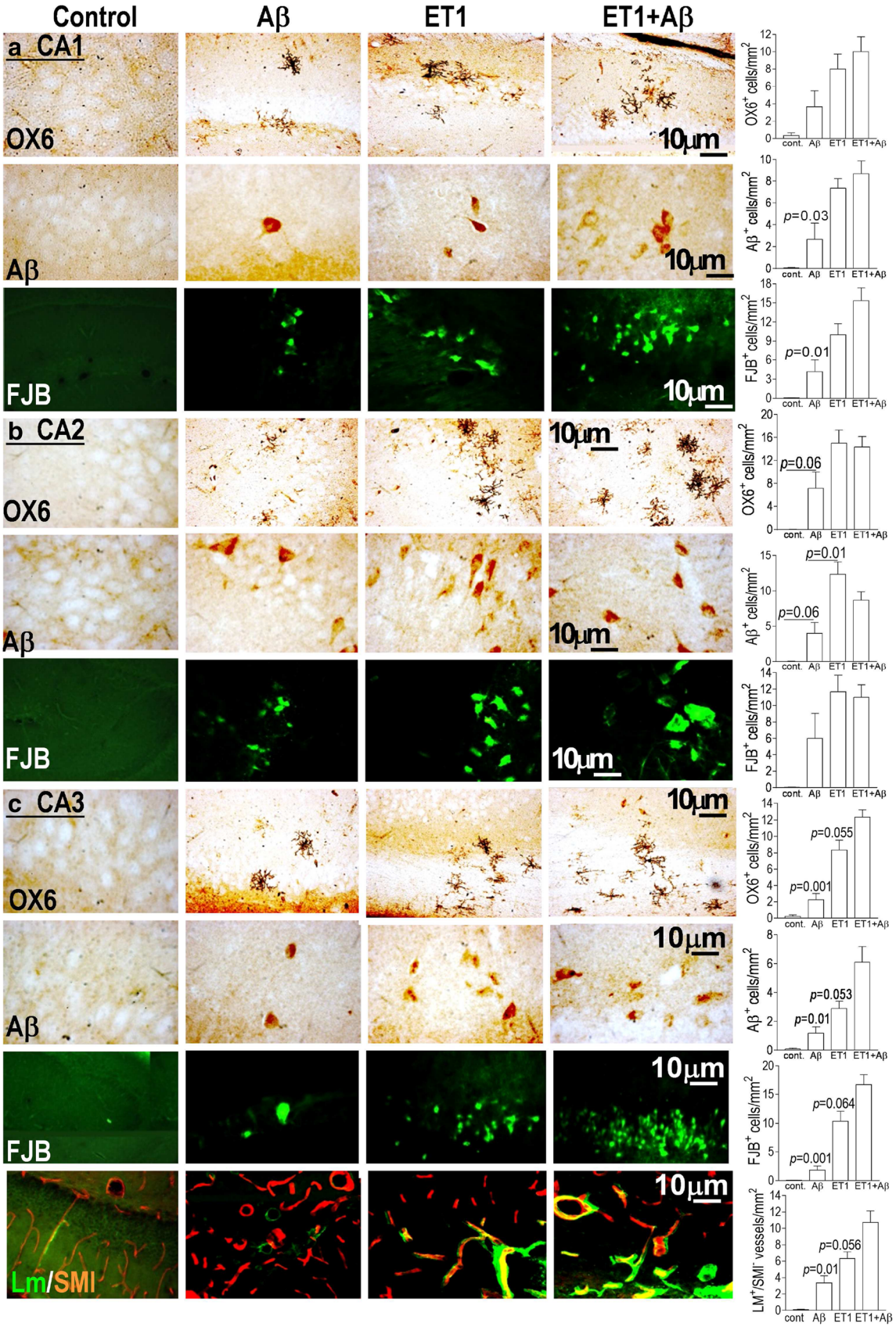
Control
Aβ
ET1
ET1+Aβ
a CA1
OX6
Aβ
FJB
b CA2
OX6
Aβ
FJB
c CA3
OX6
Aβ
FJB
Lm/SMI
10μm
OX6+ cells/mm2
Aβ+ cells/mm2
FJB+ cells/mm2
LM+/SMI vessels/mm2
cont. Aβ ET1 ET1+Aβ
p=0.03
p=0.01
p=0.06
p=0.055
p=0.001
p=0.053
p=0.064
p=0.056

◀ **Fig. 4** Cornu ammonis pathology: high-resolution images at bregma level − 3.8 mm show CA1 (a), CA2 (b), and CA3 (c) pathology in control, Aβ, ET1, and ET1 + Aβ rats. Immunostaining indicates ramified microglia (OX6), APP fragments including β-amyloid (Aβ), FJB-positive cells (FJB), laminin (Lm)- and SMI (SMI)-positive microvessels in the CA1, CA2, and CA3 regions. Plots show a quantitative analysis of OX6, Aβ, FJB, BM-laminin, and SMI immunoreactivity in the CA1, CA2, and CA3 of control, Aβ, ET1, and ET1 + Aβ rats

connecting brain regions. For instance, the first set of characteristic biochemical alteration observed was an increase in MHC II expression by ramified microglia reflecting localized hippocampal inflammation with considerably enhanced inflammation in the ET1 + Aβ rats [13]. Further, the present data reaffirms that ischemia and/or β-amyloid toxicity leads to an elevated generation of endogenous β-amyloid triggered by either Aβ 25–35 ICV injections (confirms our previous findings [13–16]), or by the heightened retention of APP in the perikarya of neuronal cells. It could also be due to the impaired transport of APP to the axons, or owing to its impaired cleavage or overexpression in neurons, astrocytes, or ramified microglia [50, 51], while our results propose it is mainly contained in neurons. Intriguingly, the formation and accumulation of APP fragments deposits within the microvessels of basal forebrain region appeared to be an initiating site to

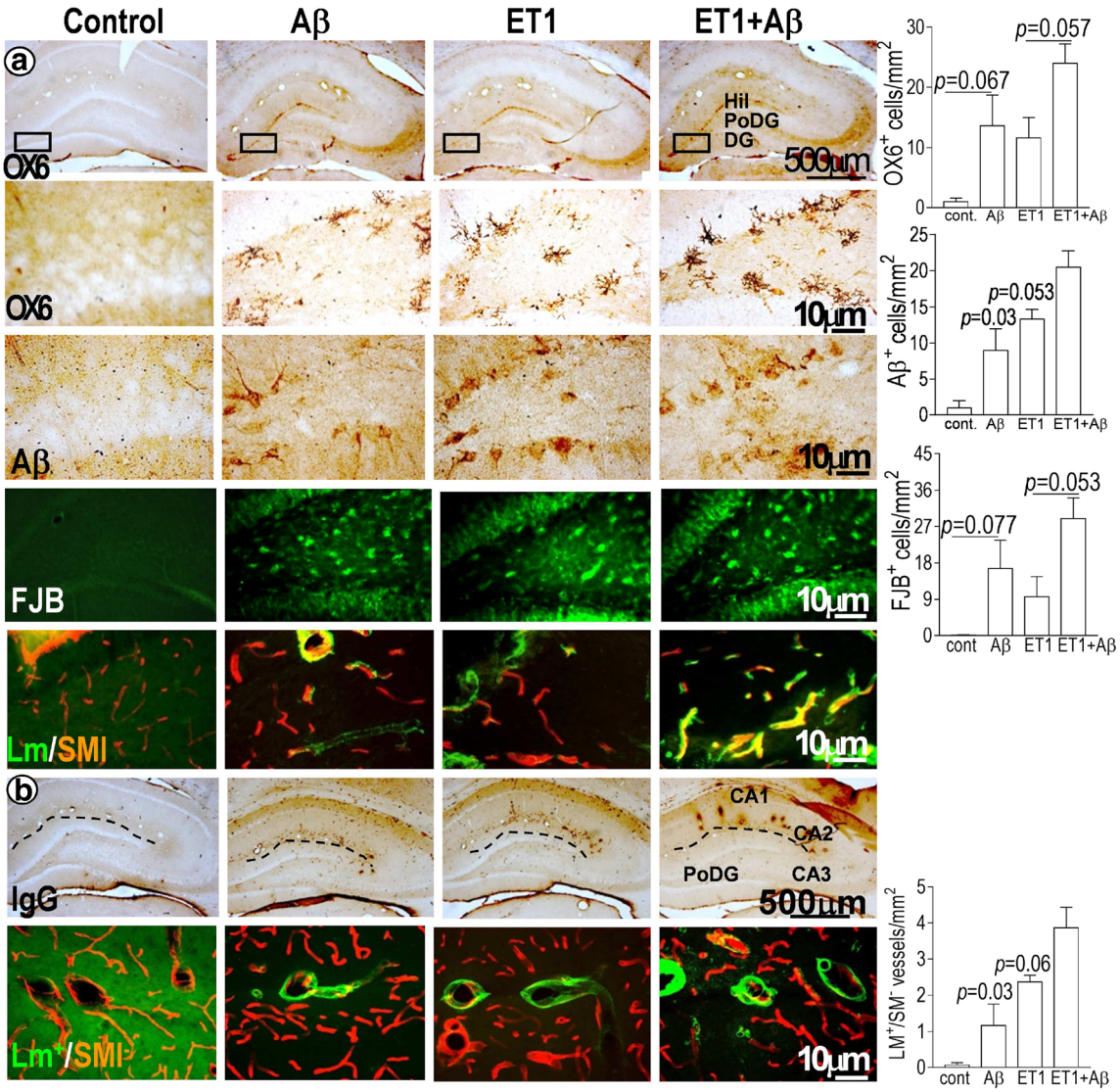


**Fig. 5** Dentate gyrus pathology: low-resolution images stained with OX6 antibody at bregma level − 3.8 mm (a) show DG pathology in control, Aβ, ET1, and ET1 + Aβ rats. The dotted rectangles indicate the region of the high magnification images. High-resolution immunostaining indicates neuroinflammation (OX6), amyloid accumulation (Aβ), cellular degeneration (FJB), BM-laminin leakage (Lm), and BBB disruption (SMI). Low-resolution images at bregma level − 3.14 mm (b) show IgG leakage through the disrupted microvessels. The dotted lines indicate the region of the high magnification images. Fluorescent immunostaining indicates BM-laminin (Lm), and SMI (SMI)-positive microvessels in the ipsilateral DG of control, Aβ, ET1, and ET1 + Aβ rats. Polymorph layer of DG (PoDG), hilus of DG (Hil), CA1, CA2, and CA3 are shown to orient the readers. Plots show quantitative analysis OX6, Aβ, FJB, BM-laminin, and SMI immunoreactivity in the DG of control, Aβ, ET1, and ET1 + Aβ rats

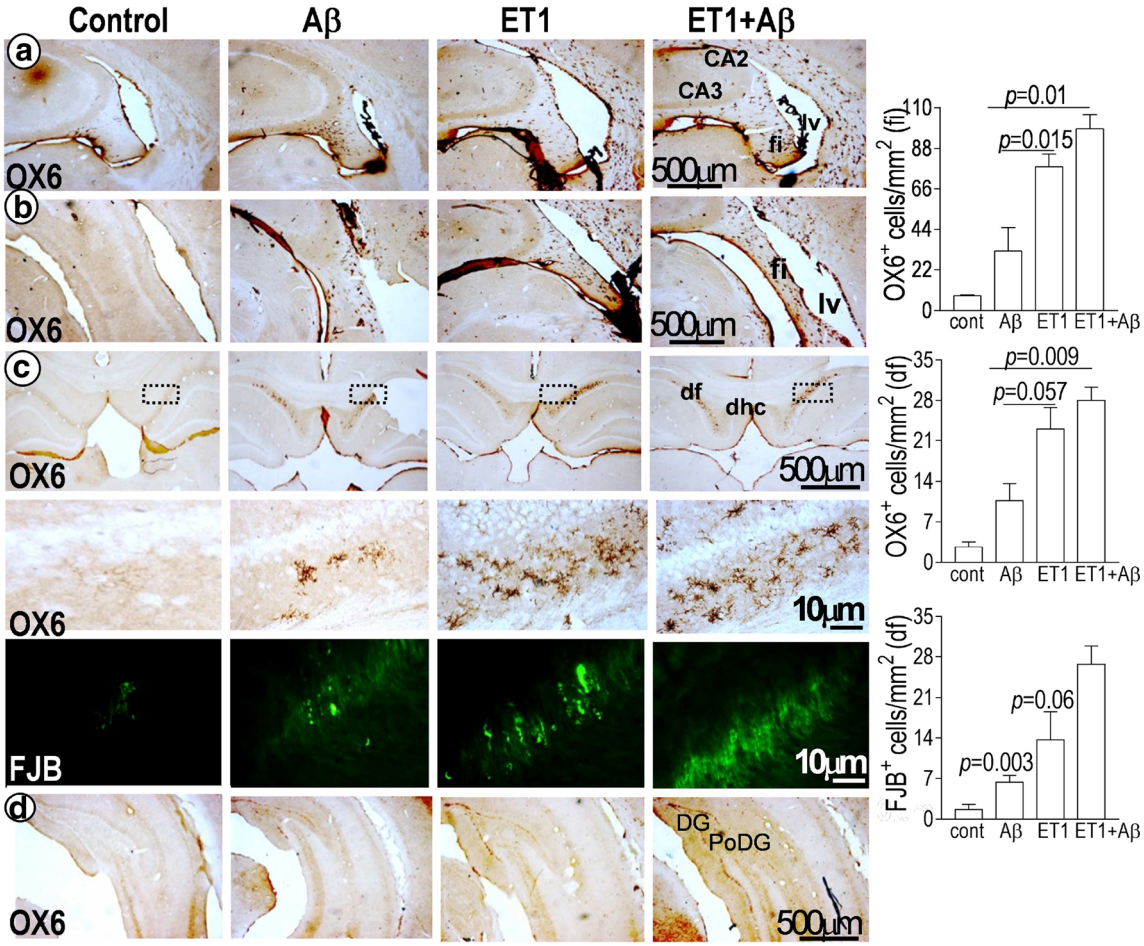


**Fig. 6** Fornix and hippocampal commissure pathology: low-resolution images at bregma levels –3.3 (a) and − 3.8 (b) mm show ramified microglia (OX6) in the fimbria of hippocampus (fi) and at bregma level − 4.52 mm show dorsal fornix (df) and dorsal hippocampal commissure (dhc) (c) of control, Aβ, ET1, and ET1 + Aβ rats. The dotted rectangles indicate the region of the high magnification images. High-resolution immunostaining indicates a dense and widespread expression of ramified microglia (OX6) and FJB-positive cells (FJB) in the ipsilateral df of control, Aβ, ET1, and ET1 + Aβ rats. CA2, CA3, and lateral ventricles (lv) are shown to orient the readers. Low-resolution images stained with OX6 antibody at bregma level − 5.8 mm (d) show extended DG pathology. Plots show quantitative assessment of immunoreactivity of OX6 in the fi and OX6 and FJB in the ipsilateral df of control, Aβ, ET1, and ET1 + Aβ rats

produce cerebral amyloid angiopathy. While DG hilar neurons and mossy fiber axons of Aβ rats showed increased APP fragments immunoreactivity, CA2 of ET1 + Aβ rats did not show any significant increase in β-amyloid as well as microglial cells compared to Aβ and ET1 rats alone. This points out that in CA2 subdivision, ischemia and Aβ toxicity do not interact to have any synergistic or additive effects.

Given that Aβ accumulation is related to the neuronal damage after brain insult [52] and that in AD, hippocampus is the main region of neurodegeneration, delayed necrotic damage is likely to contribute to the present FJB data. The appearance of FJB-positive cells (and decreased number of NeuN-positive neurons in VPM and VPL) in hippocampal-connected brain regions further indicates that the specific homeostatic mechanisms, architecture, strength, and a number of connections within the hippocampus primarily drive the pattern of degeneration. And that the ischemic injury and/or Aβ toxicity may result in cellular degeneration not only in the lesion core but also in the nonischemic areas remote from the lesion core [48, 52, 53]. In addition, different populations of hippocampal neurons displayed differential susceptibility to Aβ toxicity and/or ischemia [54]. For instance, DG, CA2, and CA3 pyramidal neurons demonstrated selective and substantial deposition of Aβ fragments but neurons in the CA1 area were relatively intact. Perhaps the toxicity induced by ET1 + Aβ was not sufficient to give metabolic stress to CA1 neurons [55].

Activated microglia are primarily involved in altering the BBB integrity and vascularization in ischemia [56] and AD [57]. Given that the onset of dementia and neurodegeneration are probably followed by the cerebrovascular alterations in AD patients [58, 59] and that Aβ

toxicity or deposits play an important role in harming the nearby microvessels [60] [61, 62] and BM [62]. The appearance of BBB loss and tortuous capillaries in all hippocampal-connected regions, a trisynaptic circuit (DG (fascia dentata and hilus), CA3), ventral pallidum (VP), anterior amygdala area (AAV), and islands of Calleja was not a surprise. Thus, not only cells but also hippocampal capillaries are vulnerable to cerebral insult.

MMP9 has a dual role after cerebral injury. The pathological role starts immediately after the injury. This role degrades BM-laminin [63] and extracellular matrix receptor β-DG to mediate BBB disruption (SMI loss) [64], inducing cytotoxic edema (as indicated by the astrocytic swelling and depolarized expression of water channel protein; AQP4), leakage of IgG and dysferlin [64, 65], (which is manifested as serum proteins leakage) with eventual loss of NeuN staining [66]. The protective role that observed almost 4 weeks after injury, in the present study, repaired the BBB by stabilizing β-DG and BM-laminin to mediate neurovascular remodeling and regeneration process [32]. While ET1 rats showed an elevated level of astrocytic MMP9 and β-DG, ET1 + Aβ rats showed comparatively decreased levels of MMP9, and microvessels with laminin meshwork still missing β-DG and SMI staining. These findings also suggest a mechanistic insight for hippocampal-related functional deficits in ET1 + Aβ rats, previously reported by us [13].

Two conclusions can be drawn from the present findings. Firstly, that an injury in any hippocampal interconnections whether distant or close is strategically destined to slowly but steadily harm hippocampus and may cause cognitive impairment sooner or later, depending on the injury severity, if not treated in a timely fashion. Secondly, the structural strategic development of the hippocampal cellular and vascular degeneration in ET1 + Aβ rats, that resembles the evolution of human dementia, is further established as an etiological link between AD and ischemia and may well be occurring in humans as ET1 is upregulated by β-amyloid in human AD brain [67]. The challenge remains to determine if curing striatal damage can lead to a reversal of the cellular and vascular degeneration in the hippocampus to provide new targets for clinical therapeutic applications, specifically when areas remotely connected to hippocampus are damaged. Promotion of timely astroglial reactivity, AQP4 expression, and MMP9 activity may serve as independent strategies for neuroprotection in comorbid cases of ischemia and AD.

**Funding Information** The funding for this project came from Canadian Institutes of Health Research (R1478A47) and a CIHR Vascular Research fellowship.

## Compliance with Ethical Standards

**Conflict of Interest** The authors declare that they have no conflict of interest.

**Abbreviations** AD, Alzheimer's disease; APP, amyloid precursor protein; Aβ, β-amyloid; ICV, intracerebroventricular; ET1, endothelin-1; ABC, avidin-biotin complex; DAB, 3,3′-diaminobenzidine tetrahydrochloride; FJB, fluorojade B

## References

1. Amaral DG, Insausti R (1990) Hippocampal formation. In: Paxinos G (ed) The Human Nervous System. Academic Press Inc, San Diego, p 711–755
2. Rosene D (1987) Cerebral cortex. In: Jones E (ed) Cerebral cortex. Plenun Pre, New York, pp. 345–456
3. Amtul Z, Atta-Ur-Rahman (2015) Neural plasticity and memory: molecular mechanism. Rev Neurosci 26:253–268
4. Amtul Z, Rahman A (2016) Neural plasticity and memory: is memory encoded in hydrogen bonding patterns? Neuroscientist 22:9–18
5. Poucet B, Benhamou S (1997) The neuropsychology of spatial cognition in the rat. Crit Rev Neurobiol 11:101–120
6. Hasselmo M (1999) Neuromodulation: acetylcholine and memory consolidation. Trends Cogn Sci 3:351–359
7. Schmidt-Kastner R, Szymas J, Hossmann KA (1990) Immunohistochemical study of glial reaction and serum-protein extravasation in relation to neuronal damage in rat hippocampus after ischemia. Neuroscience 38:527–540
8. Nikonenko AG, Radenovic L, Andjus PR, Skibo G (2009) Structural feautures of ischemic damage in the hippocampus. Anat Rec 292:1914–1921
9. Eberling JL, Jagust WJ, Reed BR, Baker M (1992) Reduced temporal lobe blood flow in Alzheimer's disease. Neurobiol Aging 13:483–491
10. Altman R, Ruttledge J (2010) The vascular contribution to Alzeheimer's disease. Clin Sci 119:407–421
11. Honig LS, Tang MX, Albert S, Costa R, Luchsinger J, Manly J, Stern Y, Mayeux R (2003) Stroke and the risk of Alzheimer disease. Arch Neurol 60:1707–1712
12. Amtul Z (2016) Why therapies for Alzheimer's disease do not work: do we have consensus over the path to follow? Ageing Res Rev 25:70–84
13. Amtul Z, Nikolova S, Gao L, Keeley RJ, Bechberger JF, Fisher AL, Bartha R, Munoz DG et al (2014) Comorbid Aβ toxicity and stroke: hippocampal atrophy, pathology, and cognitive deficit. Neurobiol Aging 35:1605–1614
14. Amtul Z, Whitehead SN, Keeley RJ, Bechberger J, Fisher AL, McDonald RJ, Naus CC, Munoz DG et al (2015) Comorbid rat model of ischemia and β-amyloid toxicity: striatal and cortical degeneration. Brain Pathol 25:24–32
15. Amtul Z, Hepburn JD (2014) Protein markers of cerebrovascular disruption of neurovascular unit: immunohistochemical and imaging approaches. Rev Neurosci 25:481–507
16. Yang J, D'Esterre CD, Amtul Z et al (2014) Hemodynamic effects of combined focal cerebral ischemia and amyloid protein toxicity in a rat model: a functional CT study. PLoS One 9:e100575
17. Amtul Z, Hill DJ, Arany EJ, Cechetto DF (2018) Altered insulin/insulin-like growth factor signaling in a comorbid rat model of ischemia and β-amyloid toxicity. Sci Rep 8:5136. https://doi.org/10.1038/s41598-018-22985-4
18. Amtul Z, Yang J, Nikolova S, Lee TY, Bartha R, Cechetto DF (2018) The dynamics of impaired blood-brain barrier restoration in a rat model of co-morbid injury. Mol Neurobiol. https://doi.org/10.1007/s12035-018-0904-4
19. Klunk W, Engler H, Nordberg A, Wang Y, Blomqvist G, Holt D (2004) Imaging brain amyloid in Alzeheimer's disease with Pittsburg Compound-B. Am Neurol 55:306–319
20. Tsenov G, Mátéffyová A, Mares P et al (2007) Intrahippocampal injection of endothelin-1: a new model of ischemia-induced

seizures in immature rats. Epilepsia 48(Suppl 5):7–13. https://doi.org/10.1111/j.1528-1167.2007.01282.x
21. Dornan WA, Kang DE, McCampbell A, Kang EE (1993) Bilateral injections of beta A(25–35) + IBO into the hippocampus disrupts acquisition of spatial learning in the rat. Neuroreport 5:165–168
22. Stepanichev MY, Moiseeva YV, Lazareva NA, Onufriev MV, Gulyaeva NV (2003) Single intracerebroventricular administration of amyloid-beta (25–35) peptide induces impairment in short-term rather than long-term memory in rats. Brain Res Bull 61:197–205
23. Magloczky Z, Freund TF (1993) Selective neuronal death in the contralateral hippocampus following unilateral kainate injections into the CA3 subfield. Neuroscience 56:317–335
24. Chan RW, Leong ATL, Ho LC, Gao PP, Wong EC, Dong CM, Wang X, He J et al (2017) Low-frequency hippocampal-cortical activity drives brain-wide resting-state functional MRI connectivity. Proc Natl Acad Sci U S A 114:E6972–E 6981. https://doi.org/10.1073/pnas.1703309114
25. Kaneko I, Morimoto K, Kubo T (2001) Drastic neuronal loss in vivo by β-amyloid racemized at Ser26 residue: conversion of non-toxic [D-Ser26]β-amyloid 1-40 to toxic and proteinase-resistant fragments. Neuroscience 104:1003–1011
26. Kubo T, Nishimura S, Kumagae Y, Kaneko I (2002) In vivo conversion of racemized βamyloid ([D-Ser26]Aβ1-40) to truncated and toxic fragments ([D-Ser26]Aβ25-35/40) and fragment presence in the brains of Alzheimer's patients. J Neurosci Res 70:474–483
27. Paxinos G, Watson C (2005) The rat brain in stereotaxic coordinates. English 7:209
28. Sternberger NH, Sternberger LA (1987) Blood-brain barrier protein recognized by monoclonal antibody. Pnas 84:8169–8173
29. Lokkegaard A, Nyengaard JR, West M (2001) Stereological estimates of number and length of capillaries in subdivisions of the human hippocampal region. Hippocampus 11:726–740
30. Schmued LC, Albertson C, Slikker W (1997) Fluoro-Jade: a novel fluorochrome for the sensitive and reliable histochemical localization of neuronal degeneration. Brain Res 751:37–46
31. Damjanac M, Bilan AR, Barrier L, Pontcharraud R, Anne C, Hugon J, Page G (2007) Fluoro-Jade® B staining as useful tool to identify activated microglia and astrocytes in a mouse transgenic model of Alzheimer's disease. Brain Res 1128:40–49
32. Cunningham LA, Wetzel M, Rosenberg GA (2005) Multiple roles for MMPs and TIMPs in cerebral ischemia. Glia 50:329–339
33. Wolburg-Buchholz K, Mack AF, Steiner E, Pfeiffer F, Engelhardt B, Wolburg H (2009) Loss of astrocyte polarity marks blood-brain barrier impairment during experimental autoimmune encephalomyelitis. Acta Neuropathol 118:219–233
34. Kajihara H, Tsutsumi E, Kinoshita A, Nakano J, Takagi K, Takeo S (2001) Activated astrocytes with glycogen accumulation in ischemic penumbra during the early stage of brain infarction: inmunohistochemical and electron microscopic studies. Brain Res 909:92–101
35. Block F, Dihne M, Loos M (2005) Inflammation in areas of remote changes following focal brain lesion. Prog Neurobiol 75:342–365. https://doi.org/10.1016/j.pneurobio.2005.03.004
36. Groenewegen HJ, Vermeulen-Vander Zee A, te Kortschot A, Witter M (1987) Organization of the projections from the subiculum to the ventral striatum in the rat. A study using anterograde transport of Phaseolus vulgaris leucoaglutining. Neuroscience 23:103–120
37. Pennartz CM, Groenewegen HJ, Lopes da Silva F (1994) The nucleous accumbens as a complex of functionality distinct neuronal ensembles: an integration of behavioural, electrophysiological and anatomical data. Prog Neurobiol 42:719–761
38. Nyakas C, Luiten PG, Balkan B, Spencer DGJ (1998) Changes in septo-hippocampal projections after lateral enthorhinal or combined enthorhinal-raphe lesions as studied by anterograde tracing methods. Brain Res Bull 21:285–293
39. Paskavitz JF, Lippa CF, Hamos JE, Pulaski-Salo D, Drachman D (1995) Role of the dorsomedial nucleous of the thalamus in Alzheimer's disease. J Geriatr Psychiatry Neurol 8:32–37
40. Xuereb JH, Perry RH, Candy JM, Perry EK, Marshall E, Bonham J (1991) Nerve loss in the thalamus in Alzeheimer's disease and Parkinson's disease. Brain 114:1363–1379
41. Carrera E, Michel P, Bogousslavsky J (2004) Anteromedian, central, and posterolateral infarcts of the thalamus: three variant types. Stroke 35:2826–2831
42. Swartz RH, Black SE (2006) Anterior-medial thalamic lesions in dementia: frequent, and volume dependently associated with sudden cognitive decline. J Neurol Neurosurg Psychiatry 77:1307–1312. https://doi.org/10.1136/jnnp.2006.091561
43. Van der Werf YD, Weerts JG, Jolles J, Witter MP, Lindeboom J, Scheltens P (1999) Neuropsycological correlates of a right unilateral lacunar thalamic infarction. J Neurol Neurosurg Psychiatry 66:36–42
44. Leranth C, Hajszan T (2007) Extrinsic afferent systems to the dentate gyrus. Prog Brain Res 163:63–84. https://doi.org/10.1016/S0079-6123(07)63004-0
45. Riekkinen PJ, LauLumaa V, Sirvio J, Soininen H, Helkala E (1987) Recent progress in the research of Alzheimer's disease. Med Biol 65:83–88
46. Di Paola M, Macaluso E, Carlesimo GA et al (2007) Episodic memory impairment in patients with Alzheimer's disease is correlated with entorhinal cortex atrophy: a voxel-based morphometry study. J Neurol 254:774–781. https://doi.org/10.1007/s00415-006-0435-1
47. Imdahl A, Hossmann K (1986) Morphometric evaluation of postischemic capillary perfusion in selectively vulnerable areas of gerbil brain. Acta Neuropathol 69:267–271
48. Uchida H, Fujita Y, Matsueda M, Umeda M, Matsuda S, Kato H, Kasahara J, Araki T (2010) Damage to neurons and oligodendrocytes in the hippocampal CA1 sector after transient focal ischemia in rats. Cell Mol Neurobiol 30:1125–1134
49. Bendel O, Bueters T, von Euler M, Ögren SO, Sandin J, von Euler G (2005) Reappearance of hippocampal CA1 neurons after ischemia is associated with recovery of learning and memory. J Cereb Blood Flow Metab 25:1586–1595. https://doi.org/10.1038/sj.jcbfm.9600153
50. Bitting L, Naidu A, Cordell B, Murphy GM (1996) Beta-amyloid peptide secretion by a microglial cell line is induced by beta-amyloid-(25–35) and lipopolysaccharide. J Biol Chem 271:16084–16089
51. Pooler AM, Arjona AA, Lee RK, Wurtman RJ (2004) Prostaglandin E2 regulates amyloid precursor protein expression via the EP2 receptor in cultured rat microglia. Neurosci Lett 362:127–130. https://doi.org/10.1016/j.neulet.2004.03.013
52. Nagasawa H, Kogure K (1990) Exo-focal postischemic neuronal death in the rat brain. Brain Res 524:196–202
53. Kirino T (1982) Delayed neuronal death in the gerbil hippocampus following ischemia. Brain Res 239:57–69
54. Harry GJ, Lefebre D (2003) Dentate gyrus: alterations that occur with hippocampal injury. Neurotoxicology 24:343–356
55. Rosenblum W (1997) Histopathologic clues to the pathways of neuronal death following ischemia/hipoxia. Neurotrauma 14:313–326
56. Lartey FM, Ahn G-O, Ali R, Rosenblum S, Miao Z, Arksey N, Shen B, Colomer MV et al (2014) The relationship between serial [18 F]PBR06 PET imaging of microglial activation and motor function following stroke in mice. Mol Imaging Biol 16:821–829. https://doi.org/10.1007/s11307-014-0745-0
57. Hopperton KE, Mohammad D, Trépanier MO, Giuliano V, Bazinet RP (2018) Markers of microglia in post-mortem brain samples from patients with Alzheimer's disease: a systematic review. Mol Psychiatry 23:177–198. https://doi.org/10.1038/mp.2017.246

58. Ujie M, Dickenstein DL, Carlow DA, Jefferies WA (2003) Blood-brain barrier permeability precedes senile plaque formation in an Alzheimer disease model. Microcirculation 10:463–470
59. Rhodin JA, Thomas T (2001) A vascular connection to Alzheimer's disease. Microcirculation 8(20):207–220
60. Kalaria RN, Bhatt SU, Lust WD, Perry G (1993) The amiloid precursor protein in ischemic brain injury and chronic hypoperfusion. Ann N Y Acad Sci 695:190–193
61. Takahashi A, Park HK, Melgar MA, Alcocer L, Pinto J, Lenzi T, Diaz FG, Rafols JA (1997) Cerebral cortex blood flow and vascular smooth muscle contractility in a rat model of ischemia: a correlative laser Doppler flowmetric and scanning electron microscopic study. Acta Neuropathol 93:354–368
62. Zarow C, Barron E, Chui HC, Perlmutter LS (1997) Vascular basement membrane pathology and Alzheimer's disease. Ann N Y Acad Sci 826:147–160
63. Leppert D, Waubant E, Galardy R et al (1995) T cell gelatinases mediate basement membrane transmigration in vitro. J Immunol 154:4379–4389
64. Agrawal S, Anderson P, Durbeej M et al (2006) Dystroglycan is selectively cleaved at the parenchymal basement membrane at sites of leukocyte extravasation in experimental autoimmune encephalomyelitis. J Cell Biol 173:1007–1019
65. Hochmeister S, Grundtner R, Bauer J, Engelhardt B, Lyck R, Gordon G, Korosec T, Kutzelnigg A et al (2006) Dysferlin is a new marker for leaky brain blood vessels in multiple sclerosis. J Neuropathol Exp Neurol 65:855–865
66. Schmidt-Kastner R, Meller D, Bellander BM, Strömberg I, Olson L, Ingvar M (1993) A one-step immunohistochemical method for detection of blood-brain barrier disturbances for immunoglobulins in lesioned rat brain with special reference to false-positive labelling in immunohistochemistry. J Neurosci Methods 46:121–132
67. Palmer JC, Barker R, Kehoe PG, Love S (2012) Endothelin-1 is elevated in Alzheimer's disease and upregulated by amyloid-β. J Alzheimers Dis 29:853–861